coatings

MDPI

Article

Photocatalytic Activity of Orchid-Flower-Shaped ZnO Nanoparticles, toward Cationic and Anionic Dye Degradation under Visible Light, and Its Anti-Cancer Potential

Siwen Zheng [1,†], Esrat Jahan Rupa [2,†], Mohan Chokkalingam [2,3,†], Xiangmin Piao [1], Yaxi Han [2], Jong Chan Ahn [2], Jinnatun Nahar [2], Byoung Man Kong [2], Gi Young Kwak [2], Jong Hak Kim [2], Deok Chun Yang [1,2], Se Chan Kang [2,*] and Yingping Wang [1,*]

[1] State Local Joint Engineering Research Center of Ginseng Breeding and Application, Jilin Agricultural University, Changchun 130118, China; siwen0717@126.com (S.Z.); pxm52_@163.com (X.P.); dcyang@khu.ac.kr (D.C.Y.)
[2] Department of Oriental Medicinal Biotechnology, College of Life Science, Kyung Hee University, Yongin-si 17104, Korea; eshratrupa91@gmail.com (E.J.R.); mohanchokkalingam.sse@saveetha.com (M.C.); navycki@gmail.com (Y.H.); jongchanahn7@gmail.com (J.C.A.); jinnatunnaharbph@gmail.com (J.N.); kong2167@naver.com (B.M.K.); kwakgiyoung8@gmail.com (G.Y.K.); jhkim@rgk.co.kr (J.H.K.);
[3] Department of Nano Electronics Materials and Sensors, Institute of Electronics and Communication Engineering, Saveetha Institute of Medical and Technical Sciences, Chennai 602105, India
* Correspondence: sckang@khu.ac.kr (S.C.K.); wangyingping@jlau.edu.cn (Y.W.)
† These authors contributed equally to this work.

check for updates

Citation: Zheng, S.; Rupa, E.J.; Chokkalingam, M.; Piao, X.; Han, Y.; Ahn, J.C.; Nahar, J.; Kong, B.M.; Kwak, G.Y.; Kim, J.H.; et al. Photocatalytic Activity of Orchid-Flower-Shaped ZnO Nanoparticles, toward Cationic and Anionic Dye Degradation under Visible Light, and Its Anti-Cancer Potential. *Coatings* **2022**, *12*, 946. https://doi.org/10.3390/coatings12070946

Academic Editor: Alexandru Enesca

Received: 30 May 2022
Accepted: 24 June 2022
Published: 4 July 2022

Publisher's Note: MDPI stays neutral with regard to jurisdictional claims in published maps and institutional affiliations.

Copyright: © 2022 by the authors. Licensee MDPI, Basel, Switzerland. This article is an open access article distributed under the terms and conditions of the Creative Commons Attribution (CC BY) license (https://creativecommons.org/licenses/by/4.0/).

Abstract: Orchid-flower-shaped ZnO nanomaterials were successfully synthesized via green synthesis and an eco-friendly approach using an aqueous extract of *Lycium chinense* fruit as a reducing and capping agent. The synthesized *Lycium chinense* orchid-flower-shaped ZnO (LC-ZnO/OF) nanoparticles (NPs) were characterized using different analytical methods through X-ray diffraction (XRD), Fourier transform infrared (FTIR) spectroscopy, transmission electron microscopy (TEM), field emission scanning electron microscopy (FE-SEM), photoelectron spectroscopy (XPS), and photoluminescence (PL). The FE-TEM analysis revealed the orchid flower shape of the nanoparticles, and the elemental composition was confirmed via XPS analysis. The photocatalytic activity of the nanoparticles was determined by the degrading cationic dye methylene blue (MB) and the anionic dye Eosin Y (EY) under visible light irradiation at (400 w) within 180 min time, where it showed a significant ability to degrade both cationic and anionic dye by almost 50%. The LC-ZnO/OF photocatalyst was also used to check the toxicity level in human cancer cells, where it exhibited remarkable cytotoxicity to the human lung cancer (A549 cell line) and human gastric adenocarcinoma hyperdiploid (AGS cell line). The present investigation suggests that LC-ZnO/OF has the potential photocatalytic ability to degrade toxic dye as well as have anti-cancer effects. These preliminary results suggest that LC-ZnO/OF could have a significant impact on the environmental and biomedical fields.

Keywords: *Lycium chinense*; zinc oxide; photocatalysis; methylene blue; Eosin Y; lung cancer cell line; AGS cell line

1. Introduction

The semiconductor nature of ZnO attracts the utmost attention of researchers due to its significant applications in devices, drug delivery, and wastewater treatment. A unique parameter of ZnO NPs is that they are highly capable of doping with groups I to V to make P-type semiconductors and enhance their photocatalytic ability [1]. Bioinspired nanomaterial synthesis has recently received considerable attention as this does not produce toxic nanoparticles, undesirable byproducts, etc. [2]. In the past decade, semiconducting nanomaterials such as TiO_2, SnO_2, GaN, CuO, Si, and ZnO have been prepared through various

methods. ZnO nanomaterials have unique properties because of their wide bandgap of 3.37 eV and their high exciting binding energy, better than several other nanomaterials. Like physical and chemical methods, ZnO nanoparticles can be prepared using nanomaterial synthesis methods—such as sol–gel, solvothermal, hydrothermal, co-precipitation, Sono-thermal, and microwave methods which require toxic chemicals to be used as a solvent; hence the biosynthesized method is examined more owing to more advantages over the chemical method [3]. Thus, alternative approaches are required to synthesize nanomaterials via green, environmentally benign, economical, energy-efficient, and facile methods. The green chemistry route produces more non-toxic and eco-friendly nanoparticles than other physio-chemical methods. The green synthesis of nanomaterials has many advantages that come from using bioinspired materials, such as plant extracts, bacteria, fungi, algae, and yeast [4–6]. In the past decade, medicinally important herbal plants have been used to synthesize nanomaterials. The plant-derived metabolites are enriched with antioxidants which act as a reducing agent to reduce the metal into stable nanoparticles. Moreover, water-soluble phytochemicals such as flavones, quinines, and organic acids are the essential components for the conversion of ZnO NPs from their precursor [7].

Removing wastes, such as organic impurities, dyes, and other water-based pollutants, from industrial materials is essential to mitigate human health concerns. The textile, leather, cosmetics, paper, printing, plastic, and rubber industries' effluent is toxic, carcinogenic, and non-biodegradable [5,8]. Organic dyes are excreted into the effluents from industries, and the toxic dyes in effluents must be degraded before being released into water streams to prevent environmental issues from developing. The photocatalytic degradation of pollutant dyes yields non-colored dye fragments, leaving behind the decolored effluent, which satisfies the requirement to decolorize effluents through wastewater treatment. Nanomaterials are usually activated to enhance the photodegradation of organic dyes under solar light. Previous reports have also shown that the visible light-assisted photocatalytic application of biosynthesized ZnO NPs showed significant degradation of dyes from wastewater [9].

In recent years, numerous studies have been developed using semiconductor-assisted photocatalysis, which has shown the ability to degrade a tremendous amount of toxic chemicals in aqueous systems. Metal oxide-assisted photocatalysts, such as zinc oxide nanomaterials, have also been previously studied due to their high surface area and photosensitivity [10].

The medicinal plant *Lycium chinense* belongs to the family *Solanaceae L. chinense*, widely harvested in subtropical countries such as China. The *Lycium* plant has become very popular as it has essential secondary metabolite compounds and nutraceutical properties [11]. *Lycium* fruits have been studied extensively for their anticancer, antioxidant, and anti-aging effects in biomedical applications [12] A bioinspired method for synthesizing metal oxide nanomaterials using various plants is promising and environmentally benign. Herbal plants have human health benefits and are used widely for developmental purposes in biomedical applications.

The biosynthesis method is a unique alternative to the chemical and physical procedures for ZnO NPs synthesis owing to its cost-effective, effectual, and desirable control particle size and time-consuming methodology. This technique is also more promising due to it being free from chemical sludge and other by-products that may be concerning during the chemical synthesis process [13].

The previous study showed that SBT-ZnO/NF nanomaterial, a green nanocatalyst synthesized from sea buckthorn fruit, exhibited high photocatalytic efficiency on different dyestuffs [14]. The plant extract contains phytochemicals such as flavonoids, tannins, alkaloids, triterpenoid saponins, and cardiac glycosides that have different biomedical properties [15]. In this study, the *L. chinense* fruit-extract-fabricated LC-ZnO/OFs were tested for their photodegradation action under visible light irradiation against organic dyes (Methylene blue, Eosin Y). The green synthesized LC-ZnO/OF was also investigated against lung cancer A549 and AGS cell lines for its toxicity.

2. Materials and Methods

2.1. Materials

The sample was collected from Han Bang Bio Laboratory, Kyung Hee University. The dried fruits were washed and cut into small pieces. Zinc nitrate hexahydrate (>98%) was collected from Sigma-Aldrich, Louis, MO, USA. NaOH (analytical grade) was purchased from Dae Jung Chemicals and Metals Co., Ltd. (Pyeontaek, Korea). All dyes were purchased from Sigma-Aldrich, Louis, MO, USA. All chemicals were used without further purification.

2.2. Cell Culture

The cell lines A549 and AGS were purchased from the Korean cell line bank (Seoul, Korea). We used Dulbecco's modified eagle's medium (DMEM) (Gibson-BRL, Grand Island, NY, USA) with 10% fetal bovine serum (FBS) and 1% penicillin/streptomycin (p/s) (WElGENE Inc., Daegu, Korea). The RPMI 1640 (Roswell Park Memorial Institute Medium) was obtained from Gen DEPOT Inc. (Barker, TX, USA).

2.3. L. chinense Extract Preparation

The fruits of *L. chinense* were appropriately rinsed with distilled water, and 10 g of *L. chinense* fine powder were ground using a grinding machine and added to a conical flask containing 100 mL distilled water before being autoclaved at high pressure for 30 min. The extract was collected through filtering using Whatman filter paper (110 mm) and centrifuged at 7000 rpm for 15 min to separate out undesirable suspended materials. The collected supernatant was stored in the refrigerator at 4 °C for two weeks to be utilized for further analysis.

2.4. Green Synthesis of ZnO Nanoparticles

LC-ZnO/OF was synthesized by the co-precipitation method using *Lycium chinense* extract. Zinc nitrate hexahydrate and NaOH were used as the precursors, and *Lycium chinense* fruit extract was used as a reducing and coating agent. A total of 10% of the *Lycium chinense* fruit extract (LC-ZnO/OFs) was taken and stirred continuously with a magnetic pellet. A further 10 mL of 0.1 M zinc nitrate salt was added dropwise to the homogeneous mixture and shifted to a hot plate. When the temperature of the mixture reached 70 °C, 15 mL of 0.2 M NaOH was added dropwise to the flask walls, stirring continuously. The synthesized LC-ZnO/OF nanoparticles were then centrifuged for purification at 10,000 rpm for 15 min. The collected NPs were purified with a sterile water wash and a methanol wash to remove excess, unwanted particles. The NPs were air-dried overnight and further utilized for the characterization studies [16].

2.5. Characterization of LC-ZnO/OF NPs

A UV-Vis spectrophotometer (UltrospecTM 2100 pro, Peabody, MA, USA) confirmed the formation of green synthesized ZnO NPs between the wavelength of 300 and 800 nm. The field emission transmission electron microscopy (FE-TEM) JEM-2100F (JEOL, Peabody, MA, USA) images demonstrated the shape and size of the metal nanoparticles, and morphological analysis was carried out using a multifunctional 200 kV operating voltage. The samples were prepared using a copper grid, where small amounts of the samples were dropped into the grid and analyzed. The extra, unwanted solution was separated from the grid using blotting paper and dried at 60 °C for 15 min in a hot-air oven. A microscopic analysis confirmed the morphology of the metal NPs. Energy-dispersive X-ray spectroscopy (EDX, JEM-2100 F JEOL, Peabody, MA, USA) supplied purity data on the NPs, and elemental mapping provided insight into the distribution of the particles into NPs, demonstrating the location and distribution of the target elements of LC-ZnO/OF [17]. A commercial HR-FESEM instrument (MERLIN (Carl Zeiss, Jena, Germany)) was utilized to characterize the surface morphology of the synthesized nanoparticles. An energy dispersive X-ray spectrometer (D8 Advance, Bruker, 28359 Bremen, Germany) was used to determine the particle sizes and nature of LC-ZnO/OF. The surface capping materials of the

LC-ZnO/OFs were determined by FTIR analysis (PerkinElmer Inc., Waltham, MA, USA) between 4000 and 450 cm^{-1}. The spectral analyses recorded were plotted as transmittance (%) versus wavenumber (cm^{-1}) [18]. X-ray photoelectron microscopy (XPS; Thermo Electron/K-Alpha, Thermo Scientific, Seoul, Korea) was employed to analyze the composition and elemental state of the nanostructures. Photoluminescence (PL) properties were examined using a Sinco Floormate FS-2 spectrofluorometer (Edinburgh Instruments Ltd., Kirkton, UK). The visible light source is a Halide lamp of 400 W from Philips company, Chennai, India.

2.6. Photocatalytic Investigation

The photodegradation activity of the biologically synthesized LC-ZnO/OFs was studied by the degradation of cationic dye (MB) and anionic dye (EY) under visible light (400 W) irradiation. The effect of the catalyst load on the photodegradation activity of MB and EY was examined by considering various amounts of catalyst, such as 20, 40, 60, and 80 mg, in 20 mL of 10 ppm dye solution. The aqueous solution of MB and EY dye with the catalyst was stirred for 30 min and further kept in the dark for one hour to analyze the chemisorption on the catalyst surface and avoid absorption error. Negligible absorption of the dye molecules was observed in the dark. After agitation, the reaction mixture was kept under visible light to start the reaction with continuous stirring. The distance between the light source and reaction mixture was fixed at 20 cm. After each interval, 2 mL of the sample was centrifuged to separate the particles. The reaction mixture was then stirred continuously during the investigation of photocatalysis. The absorbance of the clear solution was recorded using UV spectra analysis [10,19].

2.7. In Vitro Cell Cytotoxicity Assays

The cellular toxicity of LC ZnO/OF was analyzed in the A549 and AGS cell lines using a 3-(4,5-dimethyl-2thiazolyl)-2,5-diphenyl-2H tetrazolium bromide (MTT) (Life Technologies, Eugene, OR, USA) assay. The cells were cultured in Dulbecco's Modified Eagle's Medium (Gibco-BRL, Grand Island, NY, USA) containing 10% fetal bovine serum and 1% penicillin/streptomycin supplementation (WelGENE Inc., Daegu, Korea) at 37 °C with a humidified atmosphere consisting of 5% CO_2 and 95% air. The cells were then seeded at a density of 1 × 104 cells per well in a 96-well plate (Corning Costar, Lowell, NY, USA). The cells were treated with various biosynthesized LC-ZnO/OF concentrations of 0, 5, 10, 20, 50, and 100 µg/mL at 37 °C, with various time intervals of 24, 48, and 72 h, at 90% confluency. After incubation, 10 µL of MTT (5 mg/mL) in phosphate-buffered saline solution was added to each well. The wells were incubated further at 37 °C for four hours. Afterward, 100 µL of dimethyl sulfoxide was added to (insoluble) formazan crystal, turning it into a soluble, colored solution. Further to this, to determine the absorbance of different reaction mixtures, we carried out an analysis with an enzyme-linked immunosorbent assay reader (Bio-Tek Instruments Inc., Vinooski, VT, USA). The optical density of the formazan formed by untreated cells (negative control) represented 100% cell viability [20]. The experiments were performed in triplicate, with the means ± standard errors calculated.

3. Results and Discussion

3.1. Biosynthesis of Zinc Oxide Nanoparticles

The LC-ZnO/OF NPs were synthesized using *L. chinense* extract with 0.1 mM zinc nitrate salt solution at 70 °C with a hot stirrer plate using co precipitation method. After being stirred, 15 mL of 0.2 M NaOH was added dropwise to the walls of the flask, stirring continuously. The color was observed to change entirely from yellow to milky white within 25 min. The formation of ZnO NPs was confirmed by changes to the color of the reaction mixture. The total synthesis approach is shown in Scheme 1, and the blank (without *Lycium*) preparation is shown in (Supplementary Figure S1) then, the reaction mixture was kept below the magnetic stirrer for 2 h, in 70 °C stirring conditions. The white color of the sample corresponded to the formation of ZnO NPs, specifically LC-ZnO/OF NPs. After

that, ZnO paste was transferred into a ceramic crucible and kept in a muffle furnace heated to 400 °C for 2 h for the conversion of $Zn(OH)_2$ to ZnO NPs. The resultant powder was used for further characterization [4].

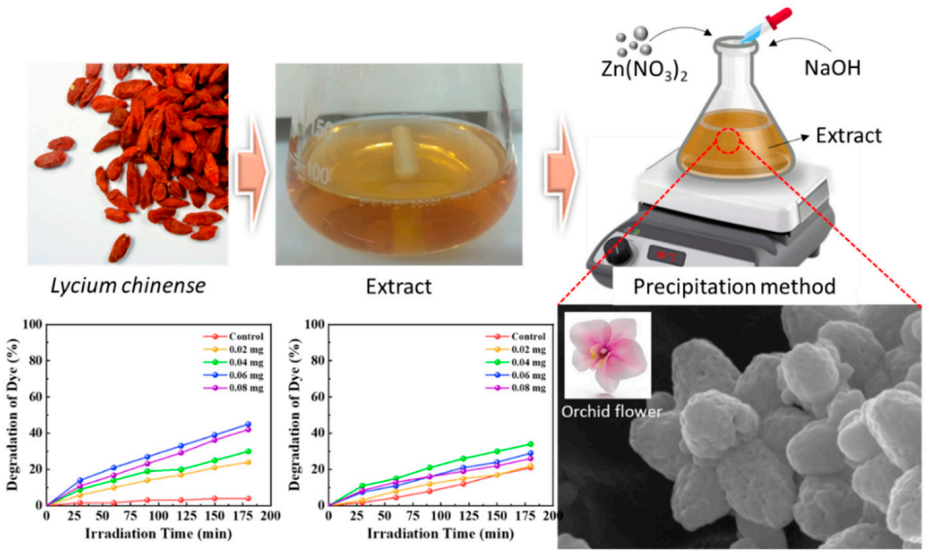

Scheme 1. Biosynthesis process of LC-ZnO/OF using *Lycium chinense* extract.

3.2. Characterization of LC-ZnO/OF NPs

The UV–visible spectrum monitored the formation and stability of LC-ZnO/OF NPs. The reactions showed the formation of LC-ZnO/OF in the reaction mixture by the color change from yellow to milky white. The *Lycium chinense* fabrication of LC-ZnO/OF NPs exhibited a characteristic UV absorption spectrum with an absorption wavelength of 390 nm, which confirm the successful formation of metal ZnO NPs, as shown in Figure 1a. The direct bandgap (Eg) calculated was 3.12 eV [14]. Also the blank sample (without *Lycium*) UV analysis shown in Supplementary Figure S1.

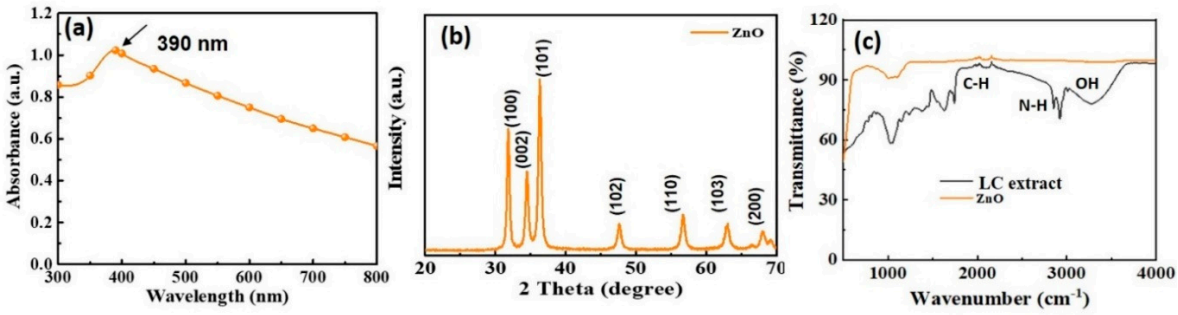

Figure 1. UV-Vis spectra of (**a**) LC-ZnO/OF and XRD spectra of (**b**) and FTIR spectra of (**c**).

3.3. XRD Analysis

The crystalline LC-ZnO/OF XRD pattern exhibited seven important and intense peaks, as indicated in Figure 1b. We observed several Bragg reflections corresponding to the crystalline structures at 2θ values of 31.82, 34.41, 36.27, 47.55, 56.61, 62.82, and 69.11; and indexed at (100), (002), (101), (102), (110), (103), and (200) sets of lattice planes, respectively.

3.4. FTIR Spectroscopic Analysis

X-ray diffraction confirmed the phase of zinc oxide nanoparticles synthesized by the bioinspired green synthesis method. FT-IR analysis was used to determine the biomolecules responsible for the reduction of Zn^{2+} and stabilization of ZnO NPs. The FT-IR analysis revealed the spectra of the sample extract before and after synthesis, as confirmed in

Figure 1c. The FTIR spectrum of the *Lycium chinense* extract showed peaks at 3274.42, 2922.36, 2852.71, 1742.13, 1628.83, and 1030.60, which shifted to 1030, with another peak around 400 to 500 for ZnO NPs samples [7]. The peak at 2924 cm^{-1} corresponded to aldehydic C–H stretching. Other bands at 1742.13 and 1628.83 corresponded to alkene (C–H) and ketone (C=O) groups, respectively. The band at 1029 cm^{-1} corresponded to the C–N stretching vibration of amine. Therefore, the synthesized ZnO NPs were surrounded by proteins and metabolites such as terpenoids with functional groups. The FTIR spectrum of LC-ZnO/OF NPs calcined at 400 °C. As a result of the calcination process, the bands in the region of 1500–3600 cm^{-1} were lost due to the removal of water molecules. These peaks disappeared entirely in the ZnO NP spectrum, clearly illustrating that the organic molecules act as capping and stabilizing agents. This suggests that the biological molecules could perform dual functions of forming and stabilizing ZnO NPs in an aqueous medium [17].

3.5. FE-SEM, TEM, and EDX Analysis

The morphology of the LC-ZnO/OF was examined using FE-SEM. The surface morphology of biosynthesized ZnO nanoparticles was studied on high-resolution FE-SEM. The SEM image appeared as an orchid-flower-shaped structure of ZnO powders, with diameters ranging from 5–200 nm (Figure 2a,b). FE-TEM studies were applied to measure the shapes and sizes of LC-ZnO/OF NPs. The shapes of LC-ZnO/OF were mostly agglomerated and polydispersed. The blank sample (without *Lycium*) shown comparatively bigger particles in FE-TEM analysis shown in Figure S2 (Supplementary Materials). The synthesized LC-ZnO/OF had diameters ranging from 200 to 50 nm (Figure 2c–f). The aggregation of particles may be due to the high surface energy of the particles. Analyses of the EDX spectra clearly showed the purity of the green synthesized LC-ZnO/OF, and elemental mapping revealed the distribution of zinc (red dot) and oxygen (green dot) atoms, as presented in Figure 2g–i. The weight and atomic proportions were approximately 83.74% (zinc), 16.26% (oxygen) and 55.76% (zinc), 44.24% (oxygen), respectively.

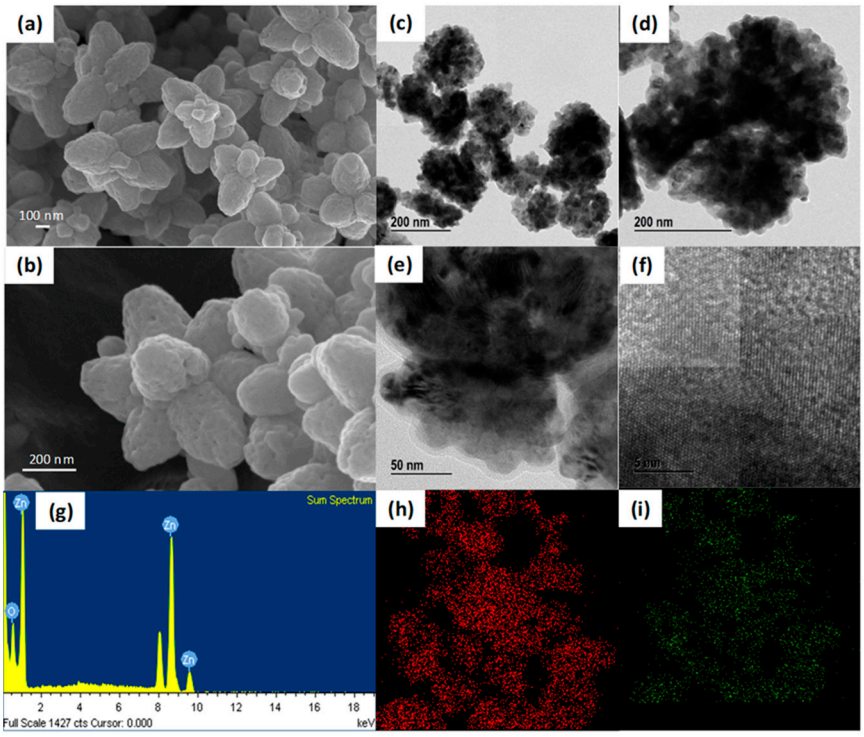

Figure 2. FE-SEM (**a**,**b**) and TEM images of LC-ZnO/OF (**c**–**f**). EDS and elemental analysis of LC-ZnO/OF (**g**–**i**).

3.6. XPS Analysis

To determine the chemical state and composition of the ZnO NPs, they were studied by XPS analysis. The XPS spectrum peak positions of the synthesized ZnO NPs for Zn ($2p^{3/2}$) and Zn ($2p^{1/2}$) were observed at around 1021.99 and 1045 eV, respectively, which were attributed to Zn^{2+} ($2p^{3/2}$) and Zn^{2+} ($2p^{1/2}$). The scans confirmed that Zn, as well as Zn^{2+}, was present in the sample. The XPS spectra for O (1s) showed a single peak located at 530.45 eV, which was attributed to the O^{2-} ions in ZnO [5], as is presented in Figure 3a–c.

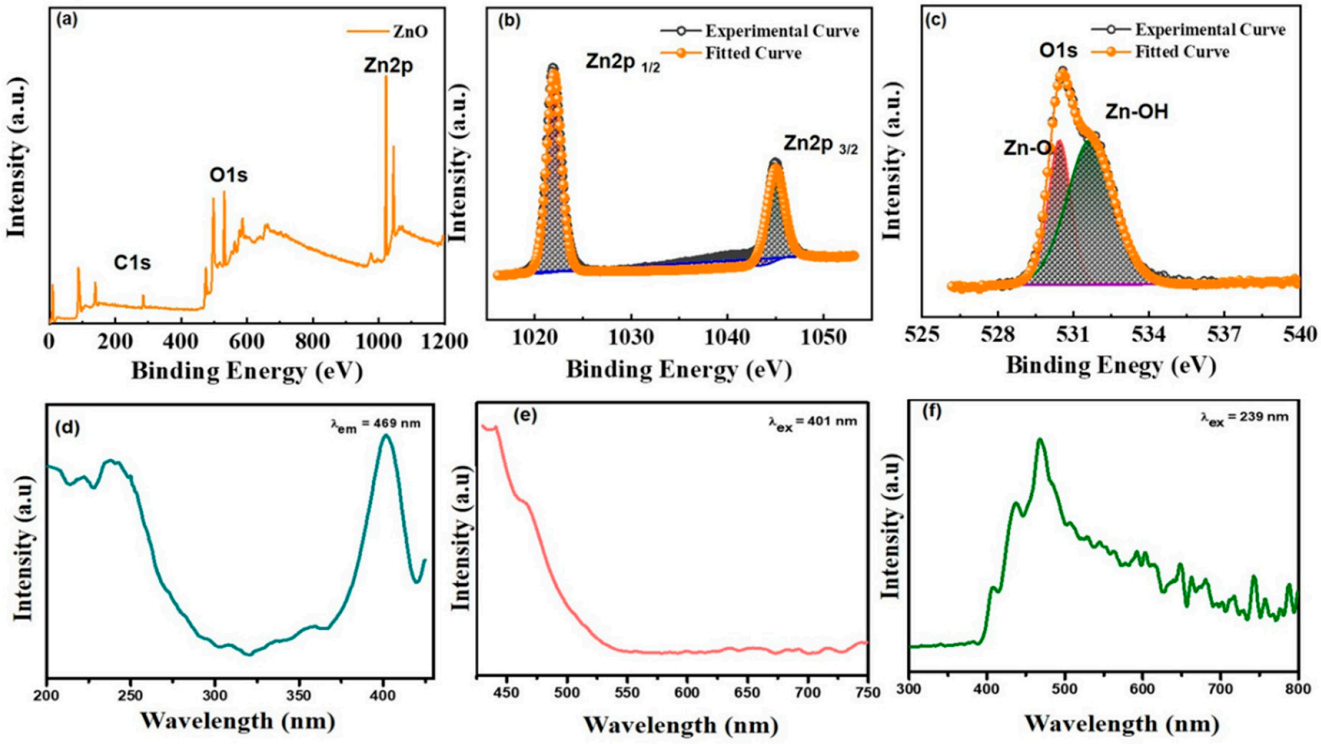

Figure 3. X-ray photoelectron spectroscopy (XPS) and PL analysis of LC-ZnO/OF. Full survey spectrum (**a**); Zn2p binding energy region (**b**); O1s binding area (**c**). Emission wavelength spectra (**d**) and Excitation wavelength (**e**,**f**).

3.7. Photoluminescence Analysis

The ZnO NPs were analyzed to better understand the functioning of photocatalysts by the photoluminescence (PL) spectra (emission and excitation wavelength spectra), as shown in Figure 3d–f. Photoluminescence spectra show emissions in both UV and visible regions when excited at 350 nm [8]. The PL excitation spectra of LC-ZnO/OF NPs were measured at an emission wavelength of 469 nm, exhibiting major peaks at 239 and 401 nm [14].

3.8. Applications of Nanoparticles

3.8.1. Photocatalytic Activity

The photocatalytic activity in the presence of biosynthesized LC-ZnO/OF NPs on cationic dye methylene blue (MB) and anionic dye Eosin Y (EY) was used to degrade under visible light (400 W) irradiation. Here, 10 ppm of MB and EY dye were examined using synthesized LC-ZnO/OF NPs under visible light irradiation with stirring. The effects of varying amounts of LC-ZnO/OF NPs on photocatalytic degradation were studied on a 10 ppm dye solution at 20–80 mg loading concentrations. The reaction mixture was stirred magnetically in the dark for half an hour to reach an adsorption-desorption equilibrium before light irradiation. The working solution was placed under the corresponding light as the next step. The visible solar spectrum was placed at a distance of 20 cm from the reaction solution. Samples collected at intervals were centrifuged at 13,500 rpm for

5 min to eliminate suspended nanoparticles. The photocatalytic activity was monitored to investigate the efficiency of LC-ZnO/OF NPs under visible light, as shown in Figure 4a–e. The UV–vis absorption results for methylene blue (MB) and EY dye were measured at 665 and 518 nm, respectively, and are shown in Figure 5a–e. Moreover, the ZnO NPs (Without *Lycium*) and *Lycium* fruit extract were also checked for degradation of both dyes (Supplementary Figure S3). The *Lycium* ZnO NPs showed better photocatalytic activity than ZnO NPs (without) and *Lycium* fruits alone. The control reactions, including MB and EY dye, were maintained without a catalyst. The performance of the optimization study with LC-ZnO/OF NPs on MB dye degradation was 45% at 0.06 g and 42% at 0.08 g, and EY dye was present at 33% at 0.06 g and 26% at 0.08 g under visible light within 3 h of irradiation, as shown in Figure 6a,b. The degradation rate increases as the amount of catalyst taken increases up to 60 mg, showing high activity, but decreases at 80 mg in cationic dye methylene blue (MB) and anionic dye Eosin Y (EY). The amount of nanoparticles increases at the same time as the adsorption number of organic dye molecules increases. As the density of particles increases, the inter-collision between the particles increases. This may result in obstruction of the light incident on the nanomaterial, and hence, the ability of the nanomaterial to release hydroxyl radicals reduces [9]. An increase in the nanoparticle load leads to an increased number of active sites available on the surface of the nanoparticles for the reaction, increasing the number of holes and hydroxyl free radicals. We observed that when the nanoparticle load increased above 80 mg, the photodegradation efficiency abruptly decreased due to the accumulation and sedimentation of the NPs on the dye. Moreover, a previous study reported that an increase in particle size and a decrease in the specific surface area resulted in a decrease in the number of active surface sites [18].

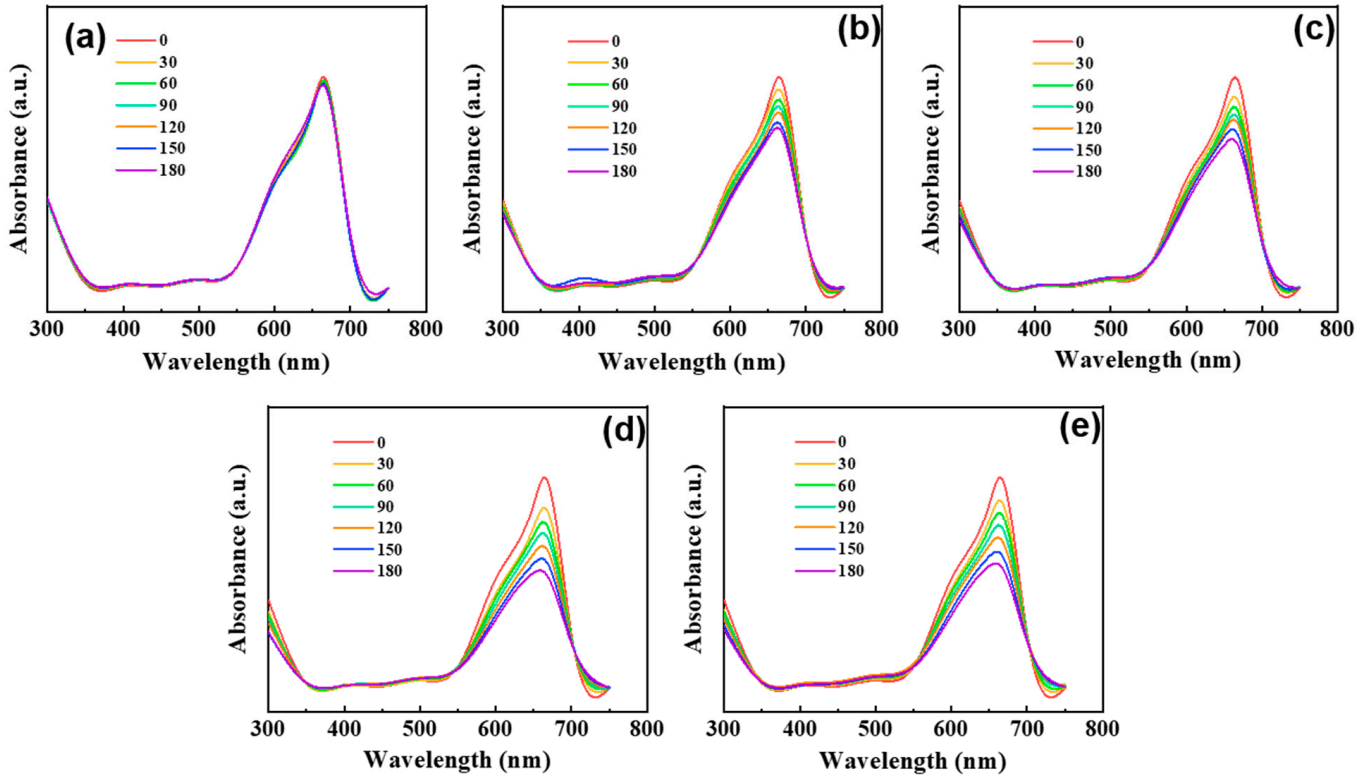

Figure 4. Absorption spectral pattern of (**a**) control and (**b**–**e**) MB during photocatalytic degradation process in the presence of LC-ZnO/OF under visible light irradiation.

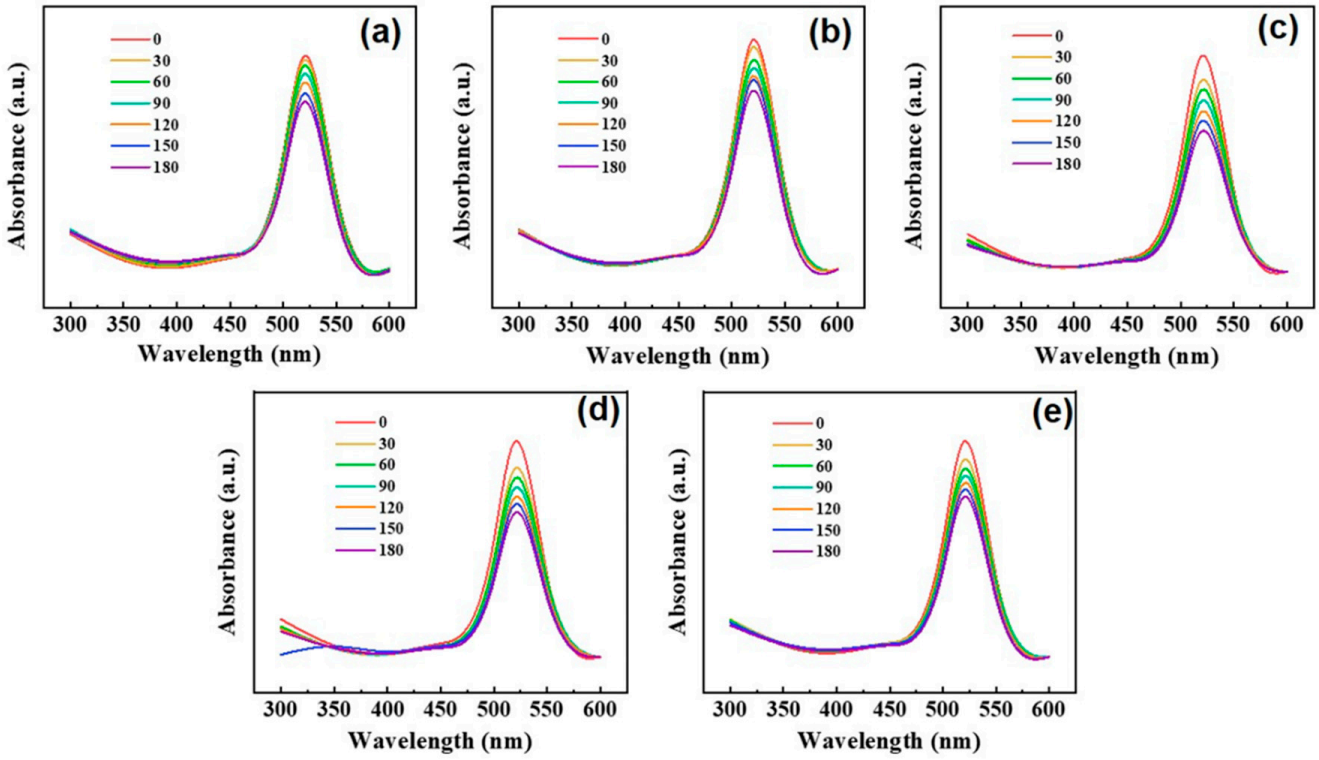

Figure 5. Absorption spectral pattern of (**a**) control and EY during photocatalytic degradation process in the presence of LC-ZnO/OF under visible light irradiation (**b**–**e**).

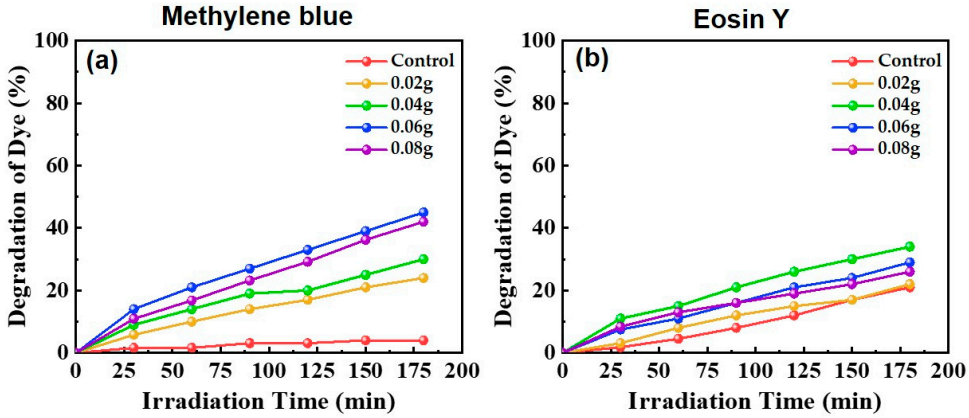

Figure 6. Dye degradation percentage of MB (**a**) and EY (**b**) with different catalyst loads under visible light.

3.8.2. Photocatalytic Degradation Kinetics

To study the catalytic efficiency of LC-ZnO/OF NPs under visible light irradiation, the degradation results were fitted to pseudo-first-order reaction kinetics using the following equation:

$$ln(C_0/C) = kt \quad (1)$$

where, k represents the rate constant (min^{-1}), C_0 represents the initial concentration of MB, and C the concentrations of MB at different time intervals. The constant rate k is equal to the slope of the fitting line. The photocatalytic dye degradation process follows the Hensel Wood pseudo-first-order reaction, with reaction rate values (kinetics value) of 0.00152, 0.00177, 0.00317, and 0.00293 min^{-1} for the MB dye and 0.00136, 0.00226, 0.00207, and 0.00155 min^{-1} for the EY dye, with LC-ZnO/OF NP loading concentrations of 0.02, 0.04, 0.06, and 0.08 g, respectively, as shown in Figure 7a,b. From the kinetics results, we

can observe that the catalyst loading concentration of 0.06 g showed the highest reaction rate of 0.00317 min^{-1} MB dye degradation, and 0.04 g showed the highest reaction rate of 0.00226 min^{-1} Eosin dye degradation. Further to these results, we observed that the optimum catalyst loading concentration was between 0.04 and 0.06 g. Moreover, we also confirmed that prepared LC-ZnO/OF NPs have a higher affinity toward the cationic dye (MB) compared to anionic dye (EY) [3,19].

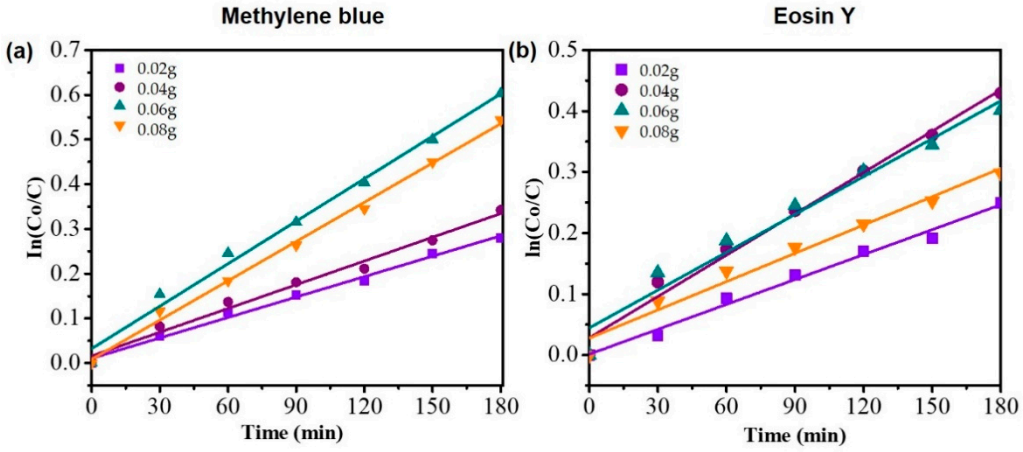

Figure 7. Kinetic study of MB (**a**) and EY dye (**b**).

3.8.3. Photocatalytic Mechanism

The photocatalytic dye degradation mechanism of ZnO is well-established. The advanced oxidation process (AOP) occurring on the catalyst's surface participates in the effective degradation of the dye molecules present in the water under light irradiation. A schematic representation of the photocatalytic mechanism shows purposeful dye degradation of the prepared LC-ZnO/OF NPs, as presented in Figure 8. On irradiating the light with sufficient energy from the photocatalyst, electrons in the valence band will excite the conduction band, causing the formation of an electron-hole pair. The holes in the valence band break down the H_2O molecules into H^+ and OH·. The electrons in the conduction band diffuse to the catalytic surface and react with oxygen molecules, forming the superoxide O_2^-·. The ROS (reactive oxygen species), OH (ad), and O_2^-· produced by AOP participate in the degradation mechanism. OH, (ad) radicals with a redox potential of 2.8 V, break down the dye molecules present in the water into safe byproducts, CO_2 and H_2O [6,20]. The dye molecules over the outer surface of the ZnO semiconductor have a tendency to split out of the C–H and C=C bond by the action of OH, hence leading to CO_2 and H_2O [20]. The overall breakdown of the dye structure in different oxidation stages finally forms the CO_2 and H_2O. The photodegradation of toxic dye mostly happens through the structural cleavage of the high molecular weight dye compound to a small compound due to the oxidation process. When the visible light source is illuminated into the ZnO semiconductor, the electron of the valance band absorbs the photon in the meantime crossing the forbidden band. The empty zone will work as a conduction band. Continuing this process, the formation of free radicals oxidizes the high molecular weight dye compound, and several oxidizing steps reduce the structural formula where some middle products were produced by cleavage of the benzene ring, such as nontoxic inorganic minerals (carbon dioxide, sulfite, nitrate, bromide, and water). Moreover, at the same time, nontoxic organic acids like acetic and oxalic can be formed [21]. The degradation of Methylene blue (cationic dye) and Eosin Y (anionic dye) causes the oxidation of dye-forming small molecular weight compounds and, finally, a breakdown of the benzene ring, forming nontoxic mineral-like carbon dioxide, sulfite, nitrate, bromide. Thus, the total mineralization process happened. In the case of Eosin Y, the disappearance of color happened due to the breakdown of polycyclic aromatic rings resulting in the formation of a small, nontoxic compound like CO_2, Br^-, Na^+ [22].

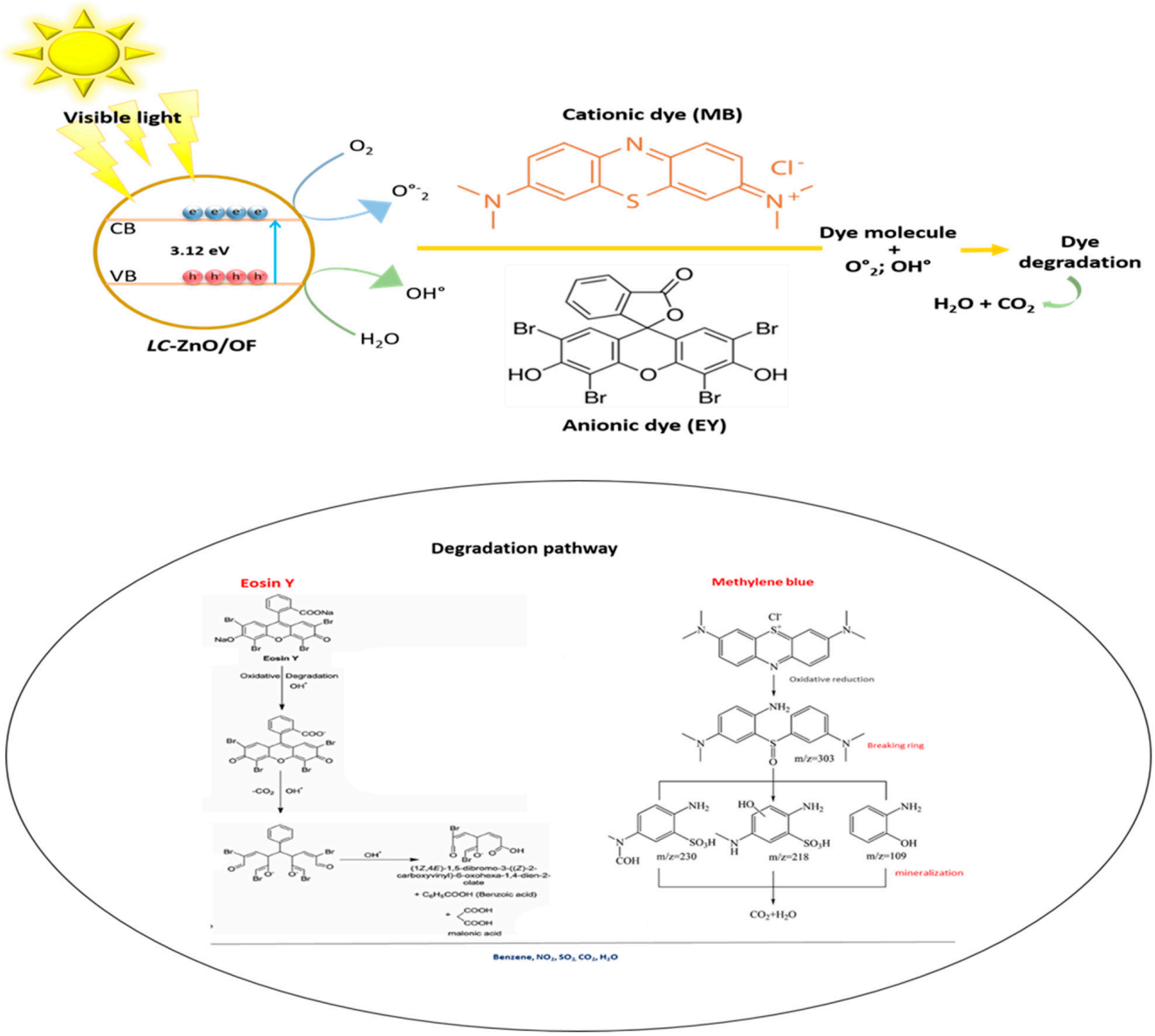

Figure 8. Schematic representation of photodegradation pathway of organic dyes using LC-ZnO/OF.

$$\text{LC-ZnO/OFNPs} + h\upsilon \rightarrow h^{+}(VB) + e^{-}(CB)$$

$$e^{-} + O_2 \rightarrow O_2{}^{-}\cdot \text{ (superoxide)}$$

$$h^{+} + H_2O \rightarrow OH\cdot + H^{+}$$

$$O_2{}^{-}\cdot + H^{+} \rightarrow HO_2\cdot$$

$$\text{Dye} + HO_2\cdot \rightarrow CO_2 + H_2O$$

$$\text{Dye} + OH\cdot \rightarrow CO_2 + H_2O$$

3.8.4. In Vitro Cytotoxicity Activity

In vitro cytotoxicity assays are essential in toxicology to elucidate the cellular response to a toxicant. The cellular viability values of A549 lung cancerous cell lines and AGS cell lines were treated with different concentrations of LC-ZnO/OF NPs, including 0, 5, 10, 20, 50, and 100 µg/mL at 37 °C, with different time points (24, 42 and 72 h) at 90% confluence. The LC-ZnO/OF NPs initiated cytotoxicity from 5 µg/mL within 24 h. After the treatment, at a 5 µg/mL concentration, 10% of the cancer cells were viable. Thus, green synthesized NPs do not lead to any significant A549 cancerous cell line toxicity at 5 µg/mL between 48 and 72 h. Interestingly, the concentration of the biosynthesized LC-ZnO/OF NPs increased from 20 µg/mL; the A549 cells lost their viability with an increase in the treatment hour at 20, 50, and 100 µg/mL, as shown in Figure 9a. We also detected that almost 90% of A549 lung cancer cells were inhibited following exposure to LC-ZnO/OF NPs at the highest concentrations (100 µg/mL) by 72 h. Moreover, the AGS cell line treatment results caused a positive impact with increased concentrations with different time point intervals [23,24]. The effect of biosynthesized LC-ZnO/OF NPs on the AGS cell line showed the significant viability of cells reduced by 60% at 72 h, as is shown in Figure 9b.

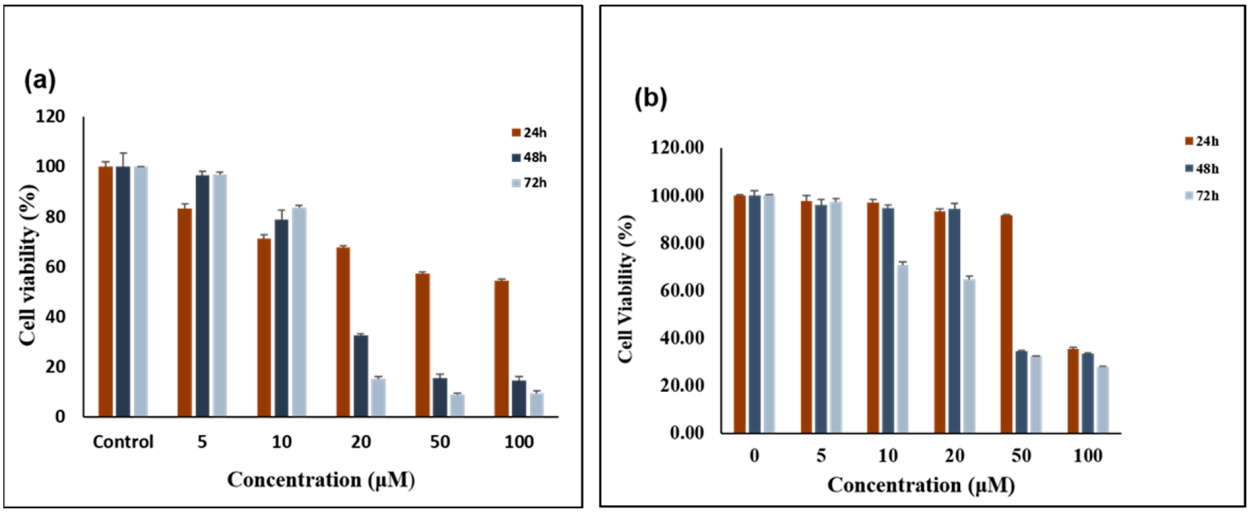

Figure 9. Cytotoxic effect of LC-ZnO/OF at different concentrations in A549 (**a**,**b**) AGS cells at 24, 48, and 72 h. Results were presented as a percentage of cell growth inhibition compared with the control.

4. Conclusions

L. chinense aqueous extract was used for green chemistry synthesis of ZnO nanoparticles, an eco-friendly method. Powder X-ray diffraction analysis confirmed the synthesized LC-ZnO/OF NPs' crystalline nature. The orchid-flower-like shape of LC-ZnO/OF NPs was found from FE-SEM. The results showed that phytochemicals in *L. chinense* extract have a good reducing ability to form nanoparticles. LC-ZnO/OF NPs can degrade MB and EY dye over time under visible light irradiation. Moreover, the biosynthesized LC-ZnO/OF nanoparticles exhibited selective cytotoxic activity against two tested cancer lines. The results revealed that green synthesized LC-ZnO/OF NPs are suitable for industrial dye wastewater treatment and biomedical applications.

Supplementary Materials: The following supporting information can be downloaded at: https://www.mdpi.com/article/10.3390/coatings12070946/s1, Figure S1: Synthesis of ZnO NPs (without adding *Lycium* fruits extract), Figure S2: The UV–visible and FE-Tem analysis of ZnO NPs (without *Lycium*), Figure S3: Comparison photocatalytic study of *Lycium* ZnO NPs, *Lycium* Extract and ZnO NPs (without *Lycium*) in both cataonic and anaonic dye methylene blue(MB) and Eosin Y(EY) degradation.

Author Contributions: Conceptualization, M.C. and E.J.R.; Data curation, M.C. and S.Z.; Funding acquisition, Y.W., S.C.K., and D.C.Y.; Investigation, X.P., Y.H., J.C.A., J.N., B.M.K., G.Y.K. and J.H.K.; Project administration, D.C.Y.; Writing—original draft, S.Z., M.C. and E.J.R. All authors have read and agreed to the published version of the manuscript.

Funding: The research was funded by Project of Science and Technology Development Plan for Jilin Province (No.20190304092YY).

Institutional Review Board Statement: Not applicable.

Informed Consent Statement: The human lung cancer cell was collected from the cell bank in Korea and was previously used for various lung cancer research at Kyung Hee University in the Hanbang bio lab.

Data Availability Statement: With the concern of the corresponding author, data can be provided.

Conflicts of Interest: The author does not have any conflict of interest.

References

1. Nguyen, L.T.; Vo, D.V.; Nguyen, L.T.; Duong, A.T.; Nguyen, H.Q.; Chu, N.M.; Nguyen, D.T.; Van Tran, T. Synthesis, characterization, and application of $ZnFe_2O_4$@ ZnO nanoparticles for photocatalytic degradation of Rhodamine B under visible-light illumination. *Environ. Technol. Innov.* **2020**, *25*, 102130. [CrossRef]
2. Azizi, S.; Namvar, F.; Mohamad, R.; Md Tahir, P.; Mahdavi, M. Facile biosynthesis and characterization of palm pollen stabilized ZnO nanoparticles. *Mater. Lett.* **2015**, *148*, 106–109. [CrossRef]
3. Rambabu, K.; Bharath, G.; Banat, F.; Show, P.L. Green synthesis of zinc oxide nanoparticles using Phoenix dactylifera waste as bioreductant for effective dye degradation and antibacterial performance in wastewater treatment. *J. Hazard. Mater.* **2021**, *402*, 123560. [CrossRef]
4. Ishwarya, R.; Vaseeharan, B.; Kalyani, S.; Banumathi, B.; Govindarajan, M.; Alharbi, N.S.; Kadaikunnan, S.; Al-anbr, M.N.; Khaledl, J.M.; Benelli, G. Facile green synthesis of zinc oxide nanoparticles using *Ulva lactuca* seaweed extract and evaluation of their photocatalytic, antibiofilm and insecticidal activity. *J. Photochem. Photobiol. B* **2018**, *178*, 249–258. [CrossRef]
5. Prasad, A.R.; Garvasis, J.; Oruvil, S.K.; Joseph, A. Bio-inspired green synthesis of zinc oxide nanoparticles using *Abelmoschus esculentus* mucilage and selective degradation of cationic dye pollutants. *J. Phys. Chem. Solids* **2019**, *127*, 265–274. [CrossRef]
6. Fowsiya, J.; Madhumitha, G.; Al-Dhabi, N.A.; Arasu, M.V. Photocatalytic degradation of Congo red using *Carissa edulis* extract capped zinc oxide nanoparticles. *J. Photochem. Photobiol. B* **2016**, *162*, 395–401. [CrossRef]
7. Singh, A.; Gautam, P.K.; Verma, A.; Singh, V.; Shivapriya, P.M.; Shivalkar, S.; Sahoo, A.K.; Samanta, S.K. Green synthesis of metallic nanoparticles as effective alternatives to treat antibiotics resistant bacterial infections: A review. *Biotechnol. Rep.* **2020**, *25*, e00427. [CrossRef]
8. Sangeeta, A.; Rimzhim, G.; Angelica, S.; Satish, K.; Subhabrata, C.; Debasish, S.; Giridhar, M. Visible light assisted improved photocatalytic activity of combustion synthesized spongy-ZnO towards dye degradation and bacterial inactivation. *RSC Adv.* **2016**, *6*, 80086.
9. Soto-Robles, C.A.; Nava, O.; Cornejo, L.; Lugo-Medina, E.; Vilchis-Nestor, A.R.; Castro-Beltrán, A.; Luque, P.A. Biosynthesis, characterization and photocatalytic activity of ZnO nanoparticles using extracts of *Justicia spicigera* for the degradation of methylene blue. *J. Mol. Struct.* **2021**, *1225*, 129101. [CrossRef]
10. Bharathi, D.; AlSalhi, M.S.; Devanesan, S.; Nandagopal, J.G.T.; Kim, W.; Ranjithkumar, R. Photocatalytic degradation of Rhodamine B using green-synthesized ZnO nanoparticles from *Sechium edule polysaccharides*. *Appl. Nanosci.* **2022**, 1–11. [CrossRef]
11. Dong, C.; Cao, C.; Zhang, X.; Zhan, Y.; Wang, X.; Yang, X.; Zhou, K.; Xiao, X.; Yuan, B. Wolfberry fruit (*Lycium barbarum*) Extract mediated novel route for the green synthesis of silver nanoparticles. *Opt. Int. J. Light Electron Opt.* **2017**, *130*, 162–170. [CrossRef]
12. Yang, L.; Liang, Q.; Zhang, Y.; Wang, S.; Yuan, F.; Wang, J. Variation of phytochemical composition of *Lycium chinense* leaves as an endemic high-value healthy resource. *Sci. Hortic.* **2021**, *281*, 109910. [CrossRef]
13. Namvar, F.; Rahman, H.S.; Mohamad, R.; Azizi, S.; Tahir, P.M.; Chartrand, M.S.; Yeap, S.K. Cytotoxic Effects of Biosynthesized Zinc Oxide Nanoparticles on Murine Cell Lines. *Evid. Based Complementary Altern. Med.* **2015**, *11*, 593014. [CrossRef]
14. Rupa, E.J.; Kaliraj, L.; Abid, S.; Yang, D.C.; Jung, S.K. Synthesis of a Zinc Oxide Nanoflower Photocatalyst from Sea Buckthorn Fruit for Degradation of Industrial Dyes in Wastewater Treatment. *Nanomaterials* **2019**, *9*, 1692. [CrossRef]
15. Selim, Y.A.; Azb, M.A.; Ragab, I.I.; El-Azim, M.H.M.A. Green Synthesis of Zinc Oxide Nanoparticles Using Aqueous Extract of *Deverra tortuosa* and their Cytotoxic Activities. *Sci. Rep.* **2020**, *10*, 3445. [CrossRef]
16. Umar, H.; Doga Kavaz, D.; Rizaner, N. Biosynthesis of zinc oxide nanoparticles using *Albizia lebbeck* stem bark, and evaluation of its antimicrobial, antioxidant, and cytotoxic activities on human breast cancer cell lines. *Int. J. Nanomed.* **2019**, *14*, 87–100. [CrossRef]
17. Ramesh, M.; Anbuvannan, M.; Viruthagiri, G. Green synthesis of ZnO nanoparticles using *Solanum nigrum* leaf extract and their antibacterial activity. *Spectrochim. Acta A Mol. Biomol. Spectrosc.* **2015**, *136*, 864–870. [CrossRef]

18. Nethravathi, P.C.; Shruthi, G.S.; Suresh, D.; Udayabhanu Nagabhushan, H.; Sharma, S.C. *Garcinia xanthochymus* mediated green synthesis of ZnO nanoparticles: Photoluminescence, photo catalytic and antioxidant activity studies. *Ceram. Int.* **2015**, *41*, 8680–8687. [CrossRef]
19. Zheng, Y.; Fu, L.; Han, F.; Wang, A.; Cai, W.; Yu, J.; Jun Yang, J.; Peng, F. Green biosynthesis and characterization of zinc oxide nanoparticles using *Corymbia citriodora* leaf extract and their photocatalytic activity. *Green Chem. Lett. Rev.* **2015**, *8*, 59–63. [CrossRef]
20. Rohilla, S.; Gupta, A.; Kumar, V.; Kumari, S.; Petru, M.; Amor, N.; Noman, M.T.; Dalal, J. Excellent UV-light triggered photocatalytic performance of ZnO. SiO2 nanocomposite for water pollutant compound methyl orange dye. *Nanomaterials* **2021**, *11*, 2548. [CrossRef]
21. Jia, P.; Tan, H.; Liu, K.; Gao, W. Synthesis, characterization and photocatalytic property of novel ZnO/bone char composite. *Mater. Res. Bull.* **2018**, *102*, 45–50. [CrossRef]
22. Hossain, A.; Rayhan, A.S.; Raihan, M.J.; Nargis, A.; Ismail, I.M.; Habib, A.; Mahmood, A.J. Kinetics of Degradation of Eosin Y by One of the Advanced Oxidation Processes (AOPs)—Fenton's Process. *Am. J. Anal. Chem.* **2016**, *7*, 863–879. [CrossRef]
23. Vidhya, E.; Vijayakumara, S.; Prathipkumar, S.; Praseetha, P.K. Green way biosynthesis: Characterization, antimicrobial and anticancer activity of ZnO nanoparticles. *Gene Rep.* **2020**, *20*, 100688. [CrossRef]
24. MubarakAli, D.; Thajuddin, N.; Jeganathan, K.; Gunasekaran, M. Plant Extract mediated synthesis of silver and gold nanoparticles and its antibacterial activity against clinically isolated pathogens. *Colloids Surf. B* **2011**, *85*, 360–365. [CrossRef]